Fluorescence mechanisms in Tm^{3+} singly doped and Tm^{3+}, Ho^{3+} doubly doped indium-based fluoride glasses

A. Brenier, C. Pedrini, and B. Moine
Laboratoire de Physico-Chimie des Matériaux Luminescents, Université Claude Bernard (Lyon I), 43 boulevard du 11 Novembre 1918, 69622 Villeurbanne CEDEX, France

J. L. Adam and C. Pledel
Laboratoire de Chimie Minérale D, Université de Rennes I, avenue du Général Leclerc, 35042 Rennes CEDEX, France
(Received 10 July 1989)

The $Tm^{3+} \rightarrow Tm^{3+}$ and $Tm^{3+} \leftrightarrows Ho^{3+}$ energy transfers have been studied in both Tm-doped and (Tm,Ho)-doped indium-based fluoride glasses over a wide temperature range for several dopant concentrations. The regime of diffusion among the Tm^{3+} ions is clearly established and the cross-relaxation $^3H_4, {}^3H_6 \rightarrow {}^3F_4, {}^3F_4$ has been proved and its efficiency calculated. The temperature dependence of the thermal equilibrium observed between the lowest excited states $^3F_4$ of Tm^{3+} and $^5I_7$ of Ho^{3+} ions in codoped glasses is explained in terms of the Boltzmann distribution of the state populations governed by efficient forward and backward energy transfers. When Tm^{3+} ions are excited in the $^3H_4$ level near 0.8 μm, it is shown that two cross-relaxation processes compete: one between Tm^{3+} ions and the other between Tm^{3+} and Ho^{3+} ions. Their efficiencies are shown to strongly depend on the relative Tm and Ho concentrations.

I. INTRODUCTION

Since their discovery 15 years ago, the heavy-metal fluoride glasses have been a subject of growing interest in many aspects. The fluorozirconate [ZrF_4-BaF_2-LaF_3-AlF_3 (ZBLA)] glasses were first synthesized[1] and then followed by many other vitreous compounds, like zirconium-free glasses based primarily on indium and barium fluorides, called BIZYT (BaF_2-InF_3-ZnF_2-YF_3-ThF_4 glasses) in this paper.[2]

One of the most interesting properties of such glasses is their weak optical absorption around 2.5 μm allowing us to consider progress in ultralow-loss optical fiber in this infrared region. But there are other important applications when these vitreous fluorides are doped by rare-earth ions which, in general, can be easily dissolved. The large optical window lying from 0.2 to 8 μm and the high emission efficiency due to a weak energy loss by multiphonon emission make these heavy-metal fluoride glasses excellent hosts for solid-state lasers emitting in the infrared region.

The optical properties of rare-earth-ion-doped fluoride glasses have been studied extensively during the past few years and a list of relevant papers can be found in Ref. 3. Previous investigations on energy-transfer processes in different Er^{3+}- and Ho^{3+}-doped glasses have shown a primary interest in the BIZYT system[4,5] and recently a spectroscopic study of Tm^{3+} ions in BIZYT has been presented.[3]

The present work deals with the excited-state dynamics of Tm^{3+} singly doped and Tm^{3+},Ho^{3+} doubly doped BIZYT. The latter system is the most interesting since it is a potential material for a Ho^{3+} laser emitting around 2 μm and pumped with currently available 0.8-μm diode lasers, since this radiation is strongly absorbed by the Tm^{3+} ions. $Tm^{3+} \rightarrow Tm^{3+}$ and $Tm^{3+} \leftrightarrows Ho^{3+}$ energy transfers are studied as a function of ion-doping levels and temperature. Their description is achieved using models constructed from rate equations and using lifetime and spectroscopic data, and their quantum efficiences are calculated.

II. EXPERIMENT

The glass used in this study has the following composition:

$$30BaF_2\text{–}30InF_2\text{–}20ZnF_3\text{–}(10-x-y)YF_3\text{–}10ThF_4\text{–}xTmF_3\text{–}yHoF_3 .$$

The method of preparation has been explained in detail in previous papers.[2]

The absorption spectra were recorded by using an ultraviolet (uv)–visible–near-infrared (NIR) spectrophotometer, model CARY 2300, spanning the wavelength range from 185 to 3152 nm, and equipped with a liquid-helium cryostat for low-temperature measurements. The emission spectra were obtained by exciting the samples with a homemade Ti (a sapphire tunable solid-state laser pumped with a cw argon laser). The fluorescence was analyzed with a Bausch&Lomb model 4 infrared no. 2 monochromator and detected with a liquid-nitrogen-

cooled PbS detector. The signal was amplified with a PAR model 186A lock-in amplifier and sent to an *X-Y* recorder. A chopper was placed on the argon laser beam to serve as a reference to the lock-in amplifier. To measure the fluorescence lifetimes, we used a powerful neodymium-doped yttrium aluminum garnet (YAG:Nd^{3+}) -pumped dye laser from QUANTEL (model DATACHROM 5000) which delivers pulses of 15 ns duration and 0.1 cm^{-1} spectral width. This laser was followed by a hydrogen Raman cell allowing infrared laser excitation up to 2 μm. The fluorescence was detected through interferential filters by a Judson Infrared, Inc. model J 10-D InSb cell cooled at liquid-nitrogen temperature and analyzed with a LeCroy 9400 Dual 125-MHz digital oscilloscope. Low-temperature lifetime measurements were performed with a cryopump model PCF 200 from L'Air Liquide, associated with a refrigerator and using helium as the cooling gas, allowing us to work from 15 to 330 K.

III. FLUORESCENCE DYNAMICS IN SINGLY DOPED Tm:BIZYT

A. Migration energy among Tm^{3+} ions in their $^3F_4$ excited state

The decays of the $^3F_4 \rightarrow {}^3H_6$ fluorescence around 1.8 μm were recorded under direct laser excitation of the $^3F_4$ level at 1.649 μm. The decays are exponential and the time constants are reported in Table I (first column) as a function of the Tm^{3+} concentration. One observes that a rapid decrease of the phenomenon can be explained by the so-called exciton annihilation process comprising a quick energy migration between Tm^{3+} ions through resonant energy transfer involving the $^3F_4$ and $^3H_6$ levels and a trapping at quenching centers (any other ion or defect to which the energy can migrate).

It is interesting to discuss here the possible regimes of donor decay which can occur in this Tm-doped BIZYT glass. Energy migration can be described either as a diffusion process or as a random walk (hopping model) and it was shown that these two models lead to similar results.[6,7] In the diffusion model, Yokota and Tanimoto[8] and then Weber[9] demonstrated in the case of dipole-dipole interaction that at long times the fluorescence of the donors decays exponentially with a time constant τ_{eff} given by

$$\frac{1}{\tau_{\text{eff}}} = \frac{1}{\tau_0} + K_D \ , \tag{1}$$

TABLE I. Lifetimes of the $^3F_4(Tm^{3+})$ and $^5I_7(Ho^{3+})$ excited states. In codoped systems (last row), the levels are thermalized and decay with the same lifetime.

mol % TmF_3 \ mol % HoF_3	0	0.5	1	2
0		10.7	10.7	10.7
0.1	12.7			
0.5	12			
2	8.3			
7	0.67	2.5	2.5	3

where τ_0 is the purely radiative lifetime of the donors and

$$K_D \simeq 4\pi D C_A \left[\frac{C_{DA}}{D}\right]^{1/4} , \tag{2}$$

where C_A is the concentration of acceptors, C_{DA} represents the donor-acceptor transfer constant, and D is the diffusion constant which is given by[7,10]

$$D = 3.375 C_D^{4/3} C_{DD} \ , \tag{3}$$

where C_D is the concentration of donors and C_{DD} is the donor-donor transfer constant. Finally one has

$$K_D \simeq V C_A C_D \tag{4}$$

with

$$V \simeq 30 C_{DD}^{3/4} C_{DA}^{1/4} \ . \tag{5}$$

The regime of donor decay described by relation (4) is known as diffusion-limited decay.

An increase in the concentration of donors produces a faster migration of energy and it was shown that for very fast diffusion the decay of the donor fluorescence is purely exponential, and then[11]

$$K_D \simeq U C_A \tag{6}$$

with U a constant depending on the type of interaction.

In the present case, the donors and acceptors are the same Tm^{3+} ions so that for K_D a linear or a quadratic C_D dependence is expected, depending on the regime of donor decay: for diffusion-limited decay,

$$\frac{1}{\tau_{\text{eff}}} - \frac{1}{\tau_0} = V C_D^2 \ , \tag{7}$$

and for very fast diffusion,

$$\frac{1}{\tau_{\text{eff}}} - \frac{1}{\tau_0} = U C_D \ . \tag{8}$$

It can be seen in Fig. 1 that Eq. (7) fits the experimental data very well with $\tau_0 = 12.725$ ms, proving that the de-

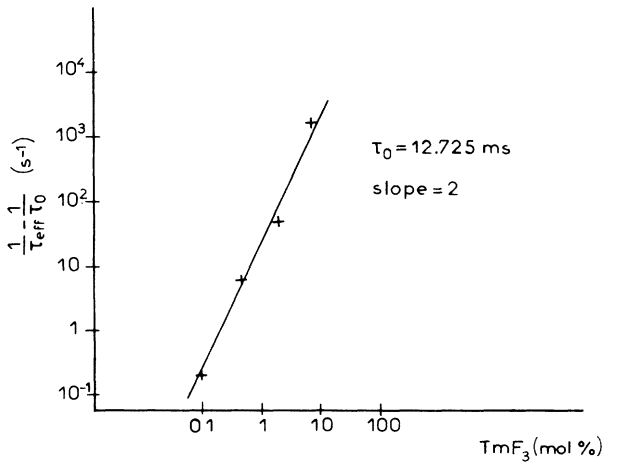

FIG. 1. Diffusion-limited decay of the $^3F_4$ excited state of Tm^{3+} ions.

cay of donor excitation is diffusion limited. Because the donor decay in the present case appears to be nearly exponential, the migration among donors is rather rapid but not very fast since relation (8) is not verified. These results are not surprising for glasses where the inhomogeneous broadening of the line shapes is large, decreasing the number of excited rare-earth impurity ions in perfect resonance, and therefore the speed of the energy migration.

B. Dynamics of the $^3H_4$ excited state

When the $^3H_4$ level is directly excited at 775 nm, it emits a fluorescence towards the ground state $^3H_4 \rightarrow {}^3H_6$ which exponentially decays. The time constants, gathered in Table II, strongly decrease when the thullium concentration increases since the $^3H_4$ lifetime varies from 1.80 ms for 0.1 mol % TmF_3:BIZYT to 2 μs for 7 mol % TmF_3:BIZYT. The $^3H_4$ dynamics can also be analyzed by studying the time dependence of the $^3F_4 \rightarrow {}^3H_6$ fluorescence. This fluorescence, decaying with the same time constant as under excitation of the $^3F_4$ level (Table I), begins with a buildup of the risetime which is characteristics of the $^3H_4$ lifetime.

The strong shortening of the $^3H_4$ lifetime emphasizes very efficient $Tm^{3+} \rightarrow Tm^{3+}$ energy transfers. The dominant process is usually assigned to the cross relaxation $^3H_4, {}^3H_6 \rightarrow {}^3F_4, {}^3F_4$ (Fig. 2) by many authors in various Tm-doped systems (see, for instance, Refs. 12–16). In our case, several experimental results support the above assignment. For example, the $^3F_4 \rightarrow {}^3H_6$ fluorescence is completely quenched in 0.1 mol % TmF_3:BIZYT because the Tm concentration is too weak to allow efficient enough cross relaxation to strongly populate the $^3F_4$ level. While the $^3H_4 \rightarrow {}^3F_4$ (near 1.5 μm) and the $^3H_4 \rightarrow {}^3H_5$ (near 2.3 μm) fluorescences are clearly detected in 0.5 mol % TmF_3:BIZYT, they are completely absent in the emission spectrum of 7 mol % TmF_3:BIZYT (Fig. 3). Indeed, the cross-relaxation process competes with the fluorescence emissions of the $^3H_4$ level and is the dominant process in Tm heavily doped crystals.

Of course, the self-quenching of the $^3H_4 \rightarrow {}^3H_6$ fluorescence can also have as its origin the exciton annihilation process previously evoked for the $^3F_4$ fluorescence quenching now involving the $^3H_4$ and $^3H_6$ levels. The concentration quenching rate is defined as

$$R_Q = \frac{1}{\tau} - \frac{1}{\tau_0} . \tag{9}$$

The quenching at maximum concentration (7% Tm) is

TABLE II. Lifetimes of the $^3H_4$ level and quantum efficiencies of the $^3H_4, {}^3H_6 \rightarrow {}^3F_4, {}^3F_4$ cross-relaxation energy transfer.

mol % TmF_3	0	0.1	0.5	2	7
τ (ms)	1.82 (extrapolated)	1.80	1.20	0.140	0.002
η_1 (%)	0	2	35	92	100

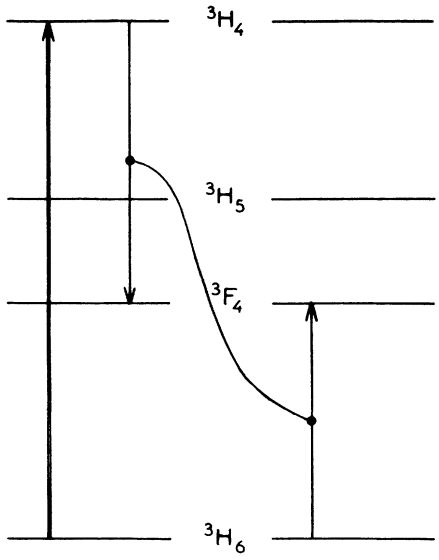

FIG. 2. Energy-level diagram of Tm^{3+} ions, showing the $^3H_4$ excitation follows by the cross-relaxation process.

5×10^5 s^{-1} for $^3H_4 \rightarrow {}^3H_6$ fluorescence compared to 1.4×10^3 s^{-1} for $^3F_4 \rightarrow {}^3H_6$ fluorescence. It is clear that the exciton annihilation contribution to the $^3H_4 \rightarrow {}^3H_6$ luminescence quenching is negligible compared to those of the cross-relaxation process, the quantum efficiency of which can be calculated by the relation

$$\eta_1 = 1 - \frac{\tau}{\tau_0} . \tag{10}$$

Table II, in which the values of η_1 are presented, shows that the down-conversion of the energy by the $^3H_4, {}^3H_6 \rightarrow {}^3F_4, {}^3F_4$ cross relaxation is totally achieved for 7 moL % TmF_3 concentration. It is interesting to note that in the present case of $^3H_4$ excitation the concentration power-law behavior is similar to the previous case. Indeed, as depicted in Fig. 4, K_D or R_Q nearly fol-

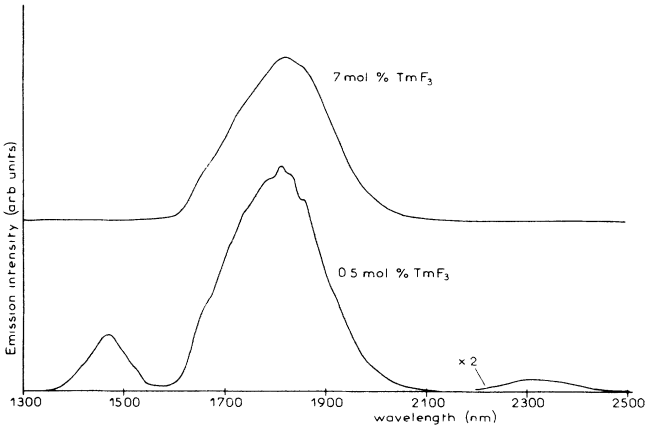

FIG. 3. Infrared-emission spectra of Tm-doped BIZYT by $^3H_4$ excitation at room temperature.

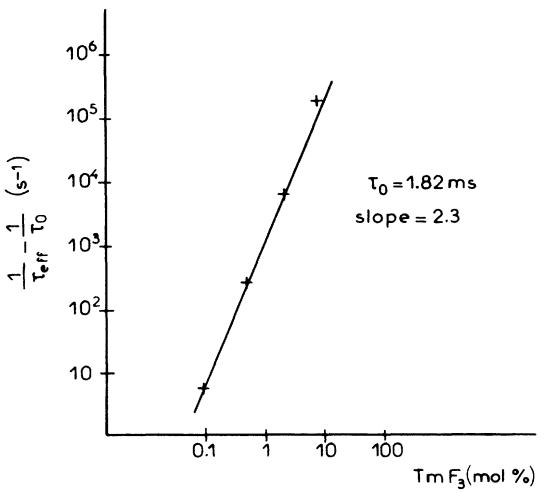

FIG. 4. Nearly diffusion-limited decay of the $^3H_4$ exited state of Tm^{3+} ions.

lows a law in VC_D^2 since the slope of the straight line is close to 2.3, indicating that the $Tm^3 \rightarrow Tm^{3+}$ energy transfer occurs in the framework of a limited-diffusion regime. As noted by Auzel,[17] the distinction between the two regimes (limited diffusion and fast diffusion) for fixed concentration is in relation to the strength of the cross-relaxation energy transfer with respect to the diffusion one; the efficient cross relaxation occurring in our Tm:BIZYT systems contributes in limiting the diffusion among Tm^{3+} ions.

IV. $Tm^{3+} \leftrightarrows Ho^{3+}$ ENERGY TRANSFERS IN DOUBLY DOPED Tm:Ho:BIZYT

The doubly doped systems investigated in the present study contain 7 mol % of thullium ions (1.3×10^{19} cm^{-3}) and various amounts of Ho^{3+} ions: 0.5 mol % (0.94×10^{18} cm^{-3}), 1 mol % (1.88×10^{18} cm^{-3}), and 2 mol % (3.67×10^{18} cm^{-3}).

A. Thermal equilibrium between $^3F_4$ (Tm^{3+}) and $^5I_7$ (Ho^{3+})

The decays of fluorescences $^3F_4 \rightarrow {}^3H_6$ of Tm^{3+} near 1.8 μm and $^5I_7 \rightarrow {}^5I_8$ of Ho^{3+} near 2 μm are first analyzed at room temperature by exciting the Tm^{3+} ions in the $^3F_4$ level with the laser radiation centered at 1.65 μm (Fig. 5). At long times, both decays are identical and exponential (the time constants gathered in Table I), indicating that the two excited states are thermalized.

At short times, just after the laser pulse and before the thermalization of the levels, the $^3F_4 \rightarrow {}^3H_6$ fluorescence of Tm^{3+} decays exponentially in a few microseconds, while the $^5I_7 \rightarrow {}^5I_8$ fluorescence of Ho^{3+} builds up with the same time constant. These results are sketched in Fig. 6 and the short time constants are shown in Table III.

These experimental data can be interpreted by the following rate equations where the notations of Fig. 5 are used:

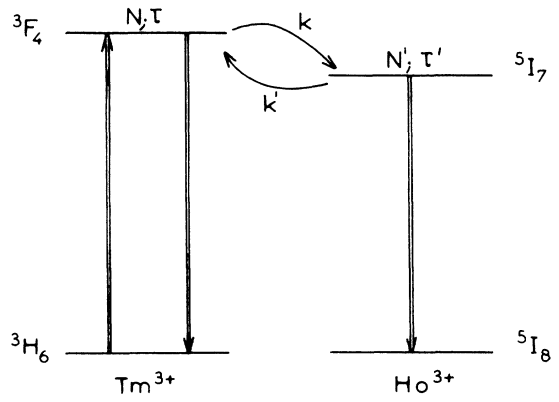

FIG. 5. Energy-level diagram of the lowest excited states of Tm^{3+} and Ho^{3+} showing the absorption and emission transitions and the forward and backward energy-transfer rates.

$$\dot{N} = -\frac{N}{\tau} - kN + k'N' ,$$
$$\dot{N} = -\frac{N'}{\tau'} - k'N' + kN , \tag{11}$$

where k and k' are the rates of forward and backward energy transfers, respectively.

The resolution of the system, by taking into account the initial conditions $N(0)=N_0$, leads to the solution given by

$$N = \alpha \exp(r_z t) + \beta \exp(r,t) ,$$
$$N' = \alpha' \exp(r,t) - \exp(r_z t) , \tag{12}$$

where α, β, and α' are constants, and where r_1 and r_2 are given by

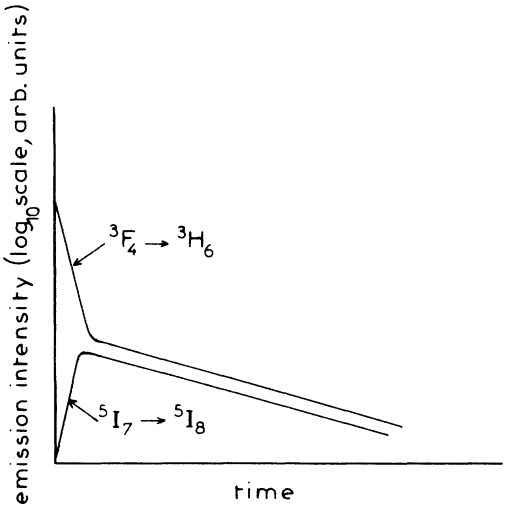

FIG. 6. Schematic representation of the time dependence of the $^3F_4(Tm^{3+})$ and $^5I_7(Ho^{3+})$ fluorescences.

TABLE III. Time constants characterizing the decays of $^3F_4(Tm^{3+})$ and $^5I_7(Ho^{3+})$ states and $^3F_4 \leftrightarrows {}^5I_7$ energy transfer rates calculated from Eqs. (18)–(20).

mol % TmF_3	mol % HoF_3	0	0.5	1	2
τ' (ms)	0		10.7	10.7	10.7
$-1/r_1$ (ms)	7		2.5	2.5	3
$-1/r_2$ (μS) ($^3F_4$ lifetime)	7	670	5.3	3.3	1.7
k (10^3 s^{-1})	7		147	237	487
k' (10^3 s^{-1})	7		41	66	101

$$r_1=\frac{1}{2}\left[-\left[\frac{1}{\tau}+k+\frac{1}{\tau'}+k'\right]+\left\{\left[\frac{1}{\tau}+k-\left[\frac{1}{\tau'}+k'\right]\right]^2+4kk'\right\}^{1/2}\right], \quad (13)$$

$$r_2=\frac{1}{2}\left[-\left[\frac{1}{\tau}+k+\frac{1}{\tau'}+k'\right]-\left\{\left[\frac{1}{\tau}+k-\left[\frac{1}{\tau'}+k'\right]\right]^2+4kk'\right\}^{1/2}\right]. \quad (14)$$

The thermalization of levels $^3F_4$ and $^5I_7$ arises because the transfer rates k and k' are much greater than the intrinsic decay rates $1/\tau$ and $1/\tau'$ of Tm^{3+} and Ho^{3+}, respectively. Taking into account these considerations, Eqs. (13) and (14) become much simpler. A Taylor-series expansion of functions r_i,

$$r_i=r_i\left[\frac{1}{\tau}=\frac{1}{\tau'}=0\right]+\frac{1}{\tau}\frac{\delta r_i}{\delta(1/\tau)}\left[\frac{1}{\tau}=\frac{1}{\tau'}=0\right]+\frac{1}{\tau'}\frac{\delta r_i}{\delta\left[\frac{1}{\tau'}\right]}\left[\frac{1}{\tau}=\frac{1}{\tau'}=0\right]+\cdots, \quad (15)$$

leads to the following results:

$$r_1=-\frac{1}{\tau}\frac{k'}{k+k}-\frac{1}{\tau'}\frac{k}{k+k'}, \quad (16)$$

$$r_2=-(k+k'). \quad (17)$$

The transfer rates k and k' are given by

$$k=-\frac{r_2}{1+\gamma}, \quad (18)$$

$$k'=k\alpha, \quad (19)$$

with

$$\gamma=-\frac{r_1+1/\tau'}{r_1+1/\tau}. \quad (20)$$

τ' is known from previous measurements in singly doped Ho:BIZYT containing the same amounts of Ho than in the doubly doped Tm:Ho:BIZYT samples presently considered,[5] and τ is the lifetime of $^3F_4$ in singly doped 7 mol % TmF_3:BIZYT. r_1 and r_2 can also be deduced from experimental data. From Eqs. (12), it is clear that r_1 represents the negative reverse of the decay time characterizing the thermalized $^3F_4$ and $^5I_7$ levels, and r_2 is the negative reverse of the time constant of the short $^3F_4$ decay or the short $^5I_7$ rise and is interpreted as the $^3F_4$ lifetime. All these experimental data and the calculated k and k' transfer rates are gathered in Table III. It should be noted that the strong decrease of the $^3F_4$ lifetime by addition of Ho^{3+} reflecting a very effective $Tm(^3F_4) \rightarrow Ho(^5I_7)$ energy transfer. The quantum efficiency is about 100% even at low Ho^{3+} concentration. One also notes that the conditions under which the formulas (18)–(20) have been derived, i.e., k and $k' \gg 1/\tau$ and $1/\tau'$ are well verified *a posteriori*. Furthermore, as it was expected, the backtransfer efficiencies are found to be small as compared with forward-transfer rates. The variations of k and k' with the Ho concentration C_A are illustrated in Fig. 7. It is satisfying to observe a linear dependence of k with C_A since this validates the use of rate equations. For the backtransfer, Tm^{3+} ions are the activators, the concentration of which is constant (7 mol % TmF_3) in the three samples studied, so that k' should not vary with Ho concentration. In fact, a weak increase of k' is observed as shown in Fig. 7. However, owing to the accuracy of the measurements (see error bars in Fig. 7), k' may be considered as nearly constant.

The temperature dependence of the $^3F_4(Tm) \leftrightarrows {}^5I_7(Ho)$

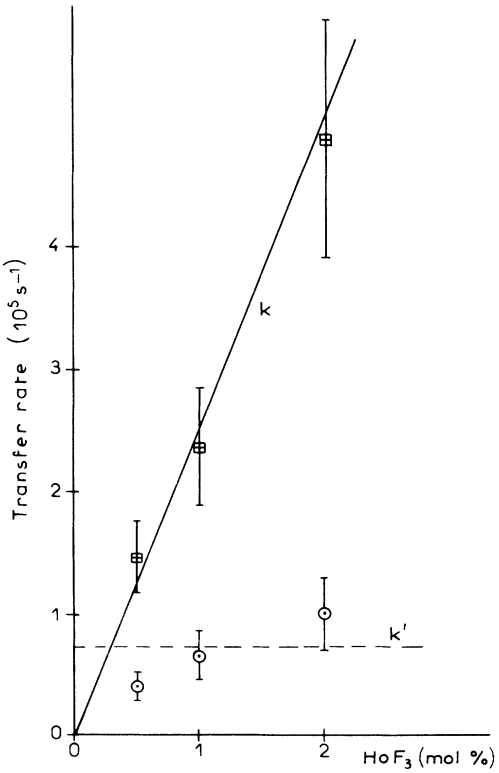

FIG. 7. Ho concentration dependence of the $^3F_4(Im^{3+}) \leftrightarrows {}^5I_7(Ho^{3+})$ transfer rates at room temperature.

energy transfers has been analyzed in the BIZYT glass containing 7 mol % Tm and 1 mol % Ho by exciting Tm ions in the $^3H_4$ level. This state has a lifetime of 2 μs in 7 mol % Tm:BIZYT so that a few microseconds after the laser pulse the fluorescence of the $^3F_4$ and $^5I_7$ levels decay with the same time constant τ''. We have demonstrated in another paper on Er:Tm:YLF (Ref. 18) that $1/\tau''$ is an average of $1/\tau$ and $1/\tau'$ balanced by the ratio of the $^3F_4$ and $^5I_7$ populations reflecting the thermal equilibrium of the levels. $1/\tau''$ can be written as

$$\frac{1}{\tau''}=\frac{\alpha}{1+\alpha}\frac{1}{\tau}+\frac{1}{1+\alpha}\frac{1}{\tau'}\ , \tag{21}$$

where $\alpha=N/N'$ is time independent, and τ,τ' are temperature independent. (The multiphonon nonradiative transitions $^3F_4\rightarrow{}^3H_6$ and $^5I_7\rightarrow{}^5I_8$ are very weak because the energy gaps $^3F_4$-$^3H_6$ and $^5I_7$-$^5I_8$ are high; 5500 cm^{-1}, and the quantum yield of the radiative transitions $^3F_4\rightarrow{}^3H_6$ and $^5I_7\rightarrow{}^5I_8$ are near unity.)

The energies of the $^3F_4$(Tm) and $^5I_7$(Ho) manifolds are obtained from low-temperature absorption measurements [Fig. 8(a)]. The absorption lines are very broad as expected in glasses where the inhomogeneous broadening is usually large, so that the energy levels can be represented as two continuous sets of levels as sketched in Fig. 9. The energy of the center of gravity of each set packet is also indicated. The most significant information which can be deduced from this energy diagram is the energy mismatch ΔE between the bottoms of the two blocks of $^3F_4$ and $^5I_7$ Stark sublevels, since ΔE can be taken as the activation energy involved in the Boltzmann distribution of the populations between the $^3F_4$ and $^5I_7$ excited states of Tm^{3+} and Ho^{3+}, respectively. The population ratio α is given by

$$\alpha=\frac{N}{N'}=\frac{C_{\mathrm{Tm}}}{C}\frac{g}{g'}\exp(-\Delta E/kT)\ , \tag{22}$$

where C_{Tm} and C_{Ho} are Tm- and Ho-ion concentrations; $g=9$ and $g'=15$ are the J degeneracies of levels $^3F_4$ and $^5I_7$.

The temperature dependence of the long-lived component τ'' is shown in Fig. 10. The solid line represents the best fit to experimental data obtained by using expressions (21) and (22), where ΔE is considered as a fitting parameter. A very good agreement between the model and the data is obtained with $\Delta E=500$ cm^{-1}, a value very close to 480 cm^{-1} deduced from low-temperature absorption measurements.

It is interesting to compare the $^3F_4$-$^5I_7$ thermal equilibrium behavior of Tm^{3+} and Ho^{3+} ions in the glass BIZYT and in the crystal $LiYF_4$. From the low-temperature absorption spectrum [Fig. 8(b)], the energy diagram deduced (Fig. 9) shows a larger ΔE of 580 cm^{-1}. This explains why the long-lived component of the $^3F_4$

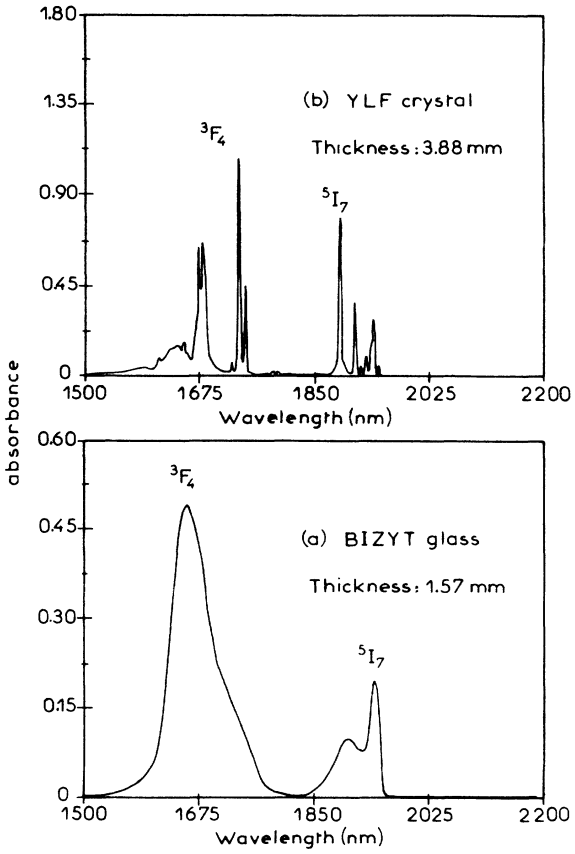

FIG. 8. Infrared-absorption spectra at $T=10$ K. (a) 7 mol % TmF_3:2 mol % HoF_3:BIZYT glass. (b) 7 mol % TmF_3:2 mol % HoF_3:$YLiF_4$(YLF) crystal.

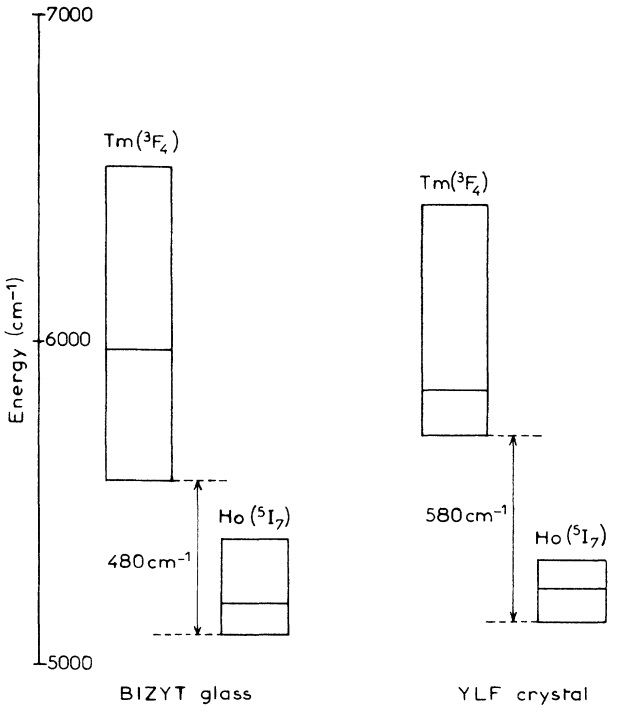

FIG. 9. Energy diagram of $^3F_4(Tm^{3+})$ and $^5I_7(Ho^{3+})$ multiplets from the absorption spectra of Fig. 8. The center of gravity of each excited state is indicated.

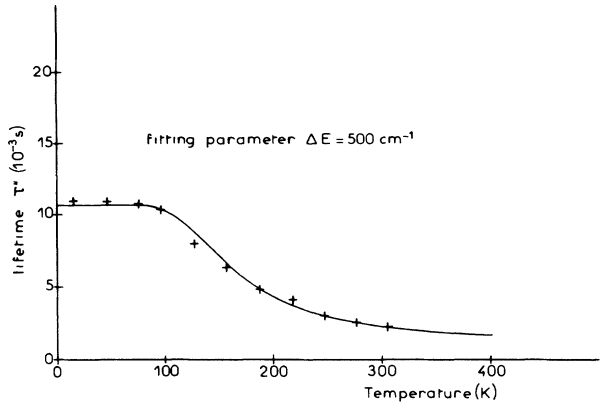

FIG. 10. Temperature dependence of the long-lived component τ'' of the $^3F_4(Tm^{3+})$ and $^5I_7(Ho^{3+})$ fluorescence in 7 mol % TmF_3:mol % HoF_3:BIZYT glass. The curve represents the best fit to experimental data obtained from Eqs. (21) and (22).

fluorescence decay resulting from the $^5I_7 \rightarrow {}^3F_4$ backtransfers is quenched at liquid-nitrogen temperature in $LiYF_4$ (Ref. 16), while in BIZYT glass it is weak but still measurable at very low temperature.

B. $^3H_4(Tm^{3+}) \rightarrow Ho^{3+}$ energy transfers

After $^3H_4$ excitation of Tm^{3+} ions, we have seen in singly doped glasses that the very efficient cross-relaxation process $^3H_4, {}^3H_6 \rightarrow {}^3F_4, {}^3F_4$ arises among Tm^{3+}. In the presence of Ho^{3+} ions, this process competes with possible direct $^3H_4(Tm^{3+}) \rightarrow Ho^{3+}$ energy transfers (Fig. 11). The variation of the $^3H_4$ lifetime with

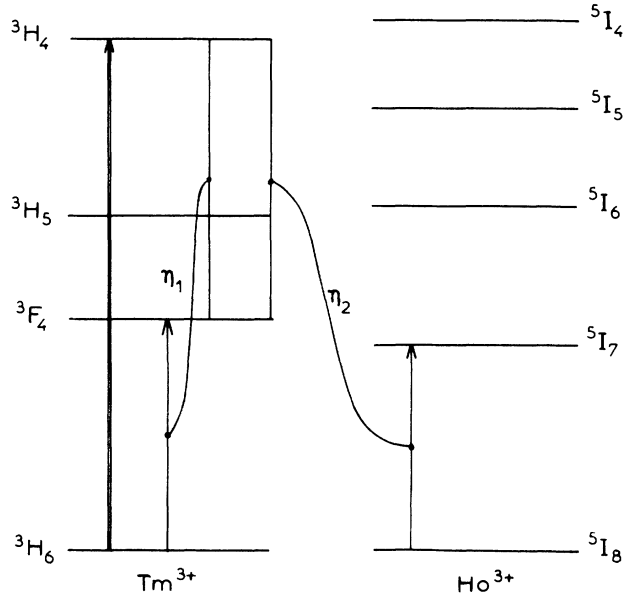

FIG. 11. Energy-level diagram of Tm^{3+} and Ho^{3+} ions where the excitation transition and the cross-relaxation processes arising between Tm^{3+} ions (efficiency η_1) and between Tm^{3+} and Ho^{3+} ions (efficiency η_2) are represented.

TABLE IV. Lifetimes of $^3H_4(Tm^{3+})$ in 7 mol % TmF_3:x mol % HoF_3:BIZYT (x=0.5,1,2) and quantum efficiency of $^3H_4(Tm^{3+}) \rightarrow Ho^{3+}$ energy transfer.

mol % HoF_3	0	0.5	1	2
$\tau(^3H_4)$ (μs)	2	1.5	1.2	0.9
η_2	0	25%	40%	55%

Ho^{3+} concentration can be studied by analyzing the risetime of the $^3F_4 \rightarrow {}^3H_6$ fluorescence rather than the decay time of the $^3H_4 \rightarrow {}^3H_6$ fluorescence which is more difficult to distinguish from the excitation laser pulse. As can be seen in Table IV, the risetime of the $^3F_4$ fluorescence which highlights the $^3H_4$ lifetime strongly shortens when the Ho concentration increases, confirming the existence of $Tm^{3+} \rightarrow Ho^{3+}$ energy-transfer processes from the $^3H_4$ level. Their efficiencies η_z can be calculated with the relation

$$\eta_z = 1 - \frac{\tau}{\tau_0} , \tag{23}$$

where τ_0 is the $^3H_4$ lifetime at 0% Ho^{3+}.

Owing to the high Tm concentration (7%), the $Tm^{3+} \rightarrow Tm^{3+}$ cross relaxation is much more efficient than the intracenter deexcitation and its efficiency η_1 is around $1-\eta_z$. Both η_1 and η_2 are indicated in Table IV.

The Tm→Ho energy transfer is probably of the cross-relaxation type, $^3H_4(Tm), {}^5I_8(Ho) \rightarrow {}^3F_4(Tm), {}^5I_7(Ho)$, which directly populates the $^5I_7$ level and short circuits the $^5I_5$ and $^5I_6$ excited states of higher energy. This assumption is supported by the fact that fluorescences originating from the $^5I_6$ level of Ho^{3+} ($^5I_6 \rightarrow {}^5I_8$ around 1.1–1.2 μm, and $^5I_6 \rightarrow {}^5I_7$ near 2.9 μm) have not been detected.

V. CONCLUSIONS

The present study of the fluorescence dynamics of Tm^{3+} and Ho^{3+} ions in indium-based fluoride glasses has established the following points.

(i) The energy when stored up in the $^3F_4$ lowest excited state of Tm^{3+} migrates through the material with a diffusion-limited regime. The diffusion is, however, fast enough to give nearly exponential fluorescence decays and provides a satisfactory account of the use of rate equations to describe the excited-state dynamics. On the other hand, the energy when stored up in the $^3H_4$ level of Tm^{3+} migrates through the glasses via the effective cross-relaxation energy transfer $Tm(^3H_4, {}^3H_6) \rightarrow Tm(^3F_4, {}^3F_4)$ arising between adjacent ions.

(ii) In Ho-doped glasses, the $Tm(^3F_4) \rightarrow Ho(^5I_7)$ energy transfer is found to be very efficient even at low Ho concentration, owing to the fast spatial energy migration among the Tm^{3+} ions at high Tm concentration (7 mol % TmF_3). The backtransfer is shown to occur even at low temperature, leading to a thermal equilibrium between the $^3F_4$(Tm) and $^5I_7$(Ho) states. Their relative populations calculated by a Boltzmann distribution are in

good agreement with experimental data.

(iii) When Tm^{3+} ions are excited in the $^3H_4$ level, the Tm→ Ho energy transfer can be achieved along two pathways; indirectly via Tm→Tm transfers (cross relaxation and diffusion), or directly via the cross-relaxation transfer $^3H_4, {}^5I_8 \rightarrow {}^3F_4, {}^5I_7$. The relative efficiences of these channels depend on the Ho activator concentration. This dynamics arises when the (Tm,Ho)-codoped laser materials are pumped with $Ga_{1-x}Al_xAs$ diode lasers emitting around 880 nm, which are now currently available.

[1]A. Lecoq and M. Poulain, Verres Refract. Pt. 1 **34**, 333 (1980).
[2]M. Poulain and J. Lucas, Verres Refract. Pt. 1 **32**, 505 (1978); A. Bouaggad, G. Fonteneau, and J. Lucas, Mater. Res. Bull. **22**, 685 (1987).
[3]C. Guery, J. L. Adam, and J. Lucas, J. Lumin. **42**, 181 (1988).
[4]J. L. Adam, C. Guery, J. Rubin, B. Moine, G. Boulon, and J. Lucas, Mater. Sci. Forum **19-20**, 573 (1987).
[5]B. Moine, A. Brenier, and C. Pedrini, IEEE J. Quantum Electron **QE-25**, 88 (1989).
[6]R. K. Watts, in *Optical Properties of Ions in Solids,* edited by B. Di Bartolo (Plenum, New York, 1975), p. 307.
[7]B. Di Bartolo, in *Energy Transfer Processes in Condensed Matter,* edited by B. Di Bartolo (Plenum, New York, 1984), p. 103.
[8]M. Yokota and O. Tanimoto, J. Phys. Soc. Jpn. **22**, 779 (1967).
[9]M. J. Weber, Phys. Rev. B **4**, 2932 (1971).
[10]M. V. Artamova, C. M. Briskim, A. I. Burshtein, L. D. Zusman, and A. G. Skleznev, Zh. Eksp. Teor. Fiz. **62**, 863 (1972) [Sov. Phys.—JETP **35**, 457 (1972)].
[11]R. K. Watts and H. J. Richter, Phys. Rev. B **6**, 1584 (1972).
[12]B. M. Antipenko, Sov. J. Techn. Phys. **29**, 228 (1984).
[13]E. W. Duczynski, G. Huber, V. G. Ostroumov, and I. A. Scherbakov, Appl. Phys. Lett. **48**, 1562 (1986).
[14]T. Y. Fan, G. Huber, R. L. Byer, and P. Mitzscherlich, Opt. Lett. **12**, 678 (1987).
[15]G. J. Kintz, L. Esterowitz, and R. Allen, Electron. Lett. **23**, 616 (1987).
[16]A. Brenier, J. Rubin, R. Moncorge, and C. Pedrini, J. Phys. (Paris) **50**, 1463 (1989).
[17]F. Auzel, in *Radiationless Processes,* edited by B. Di Bartolo (Plenum, London, 1980), p. 213.
[18]A. Brenier, R. Moncorge, and C. Pedrini (unpublished).